

Probing For Non-Gravitational Long-Range Dark Matter Interactions

M.P. Ross,¹ E.A. Shaw,¹ C. Gettings,¹ S.K. Apple,¹ I.A. Paulson,¹ and J.H. Gundlach¹

¹*Center for Experimental Nuclear Physics and Astrophysics,
University of Washington, Seattle, Washington 98195, USA*

Dark matter remains a mystery in fundamental physics. The only evidence for dark matter's existence is from gravitational interactions. We constructed a precision torsion balance experiment to search for non-gravitational, long-range interactions between ordinary matter in our lab and the Milky Way's dark matter. We find no evidence of such interaction and set strict upper bounds on its strength. These results suggest that dark matter only interacts gravitationally over long distances and constrains a variety of dark matter theories.

Introduction - Dark matter has remained a persistent mystery in fundamental physics. Decades of cosmological observations – including galactic rotation curves [1], large-scale structure surveys [2, 3], and measurements of the cosmic microwave background [4] – have established that dark matter constitutes approximately 26% of the universe's mass-energy content, far greater than the 5% contribution from ordinary matter. [4] The luminous matter of the Milky Way galaxy is embedded in a halo of dark matter that makes up most of the galaxy's mass. [5] Despite this apparent abundance, the true identity of dark matter remains elusive and it is still unknown whether dark matter interacts in another way beyond gravity.

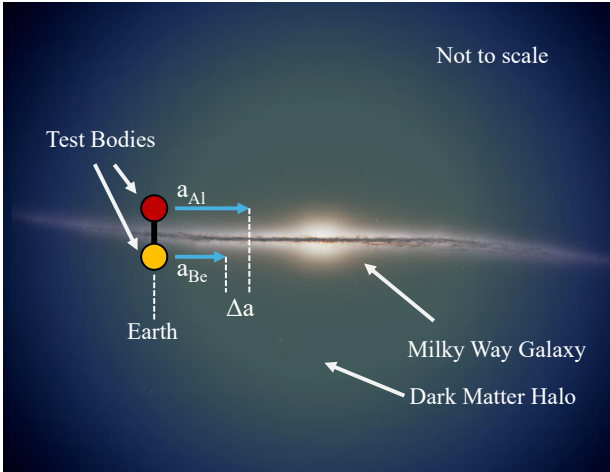


FIG. 1. A schematic of the experimental setup in the galactic frame. The experiment searches for differential accelerations of two different materials towards the dark matter in the Milky Way galaxy. Adapted from ESA/Gaia/DPAC, Stefan Payne-Wardenaar. [6]

The prevailing paradigm envisions dark matter as a new class of non-baryonic, weakly-interacting particles [7, 8]. However, every effort at detecting and producing particle dark matter has come up empty. [9] This invites serious consideration of nontraditional possibilities including: primordial black holes [10], sterile neutrinos [11], and entirely undiscovered phenomena.

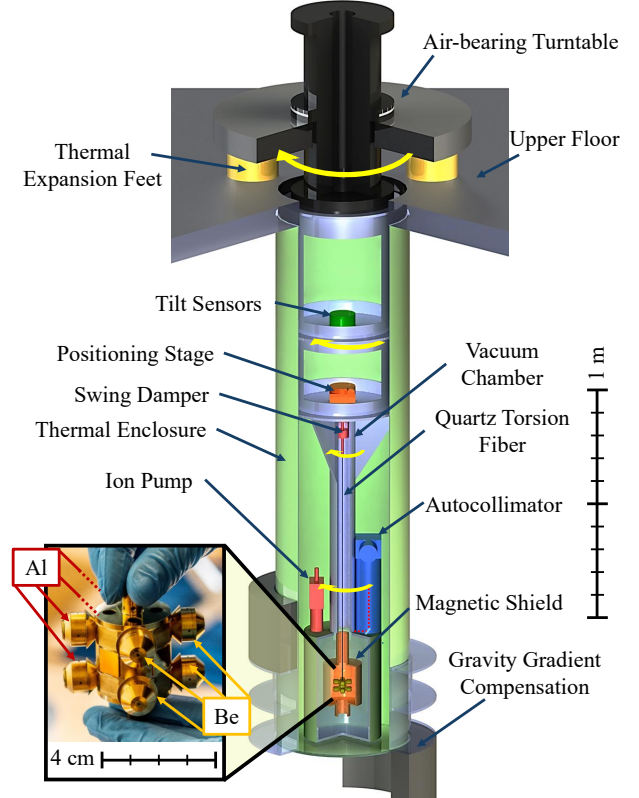


FIG. 2. Schematic of the rotating torsion balance apparatus with embedded picture of the pendulum held before installation. The thermal shields, vacuum chamber, and magnetic shields have been cut away to show the torsion balance held inside. The torsion pendulum has four test bodies made of aluminum and four of beryllium in a dipole orientation. The pendulum is suspended by a quartz torsion fiber attached to a magnetic swing damper whose position can be actuated by the positioning stage. The vacuum chamber, torsion balance, autocollimator, and magnetic shield are suspended from the air-bearing turntable. The rotating tilt sensors are used to level the turntable by actuating the thermal expansion feet. The angle of the pendulum relative to the vacuum chamber is measured by the autocollimator.

We constructed a laboratory experiment to search for non-gravitational, long-range interactions between ordinary matter and the Milky Way's dark matter. We mea-

sured the acceleration difference between two different materials directed towards the center of the Milky Way galaxy, as shown in Figure 1. Resolving such minuscule differential accelerations required development of an ultra-sensitive torsion balance apparatus.

Apparatus - Torsion balances are highly sensitive mechanical systems that have long been used for fundamental physics experiments. [12] They are formed by a pendulum suspended from a thin fiber that acts as a weak torsional spring.

Our torsion pendulum consisted of a light-weight frame that held four test bodies made of beryllium and four made of aluminum. This formed a composition dipole oriented perpendicular to the torsion fiber (Figure 2). The pendulum was designed with a high degree of symmetry to minimize coupling to gravitational gradients and other known interactions, such as electrostatics. The external surfaces were coated with gold to reduce surface charges. The pendulum was suspended from a 22- μm thick, 1-m long fused quartz fiber [13], which gave the balance a torsional period of 1472 seconds and a ring down time of ~ 2 years.

The torsion balance was held inside a vacuum chamber maintained at < 0.2 mPa by an ion pump. At low frequencies (< 1 mHz), internal thermal noise [14] of the torsion fiber limited the performance of the balance. The

angle of the pendulum relative to the vacuum chamber was measured with an autocollimator. The autocollimator reflected a laser beam off one of the four mirrors attached to the pendulum. Table I displays some of the relevant parameters of the torsion balance apparatus.

To avoid slowly varying noise (i.e. $1/f$ -noise), we modulated the signal of interest by suspending the entire apparatus from a high-precision air-bearing turntable that was set to continuously rotate at 2.85 mrad/s ($2/3$ of the torsional resonance frequency). The turntable was located on the upper floor of our laboratory with the rest of the apparatus extending to the floor below. The turntable's angle encoder was locked to an external clock which maintained a constant rotation rate by varying the torque applied with an eddy current motor. [15]

Misalignment of the rotation axis of the turntable and the torsion fiber axis (i.e. local vertical) can cause a parasitic once per turntable-revolution modulation by varying the torsion fiber attachment, translating the autocollimator beam, and/or changing the electrostatic environment around the pendulum. Such a modulation would not be correlated with the dark matter signal but could be a significant noise source. To mitigate this, we devised a control system that processed the signal from a pair of co-rotating tilt sensors to control the temperature of two of the three feet on which the turntable rests.

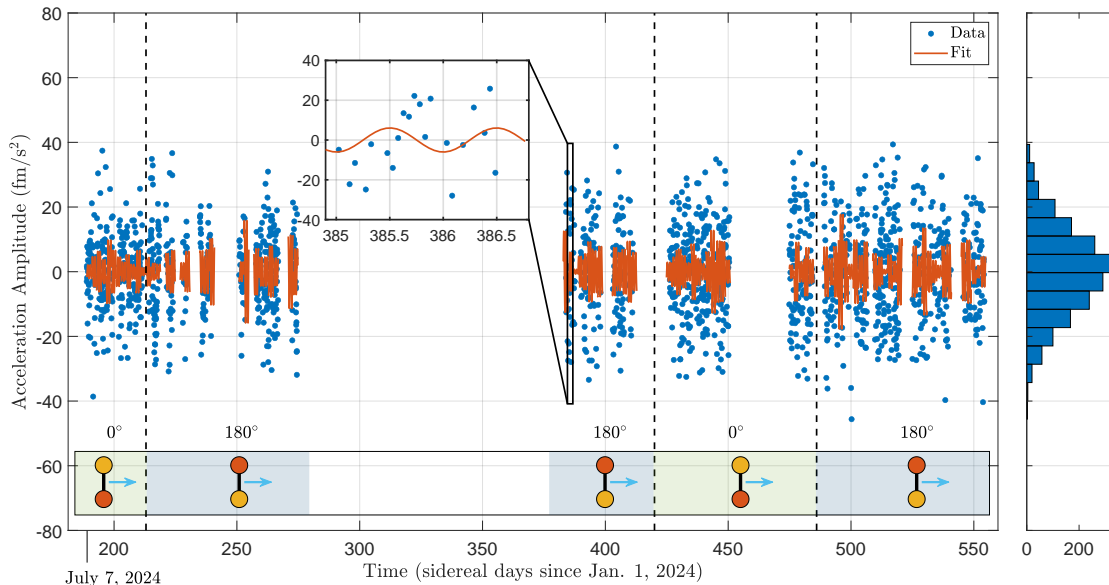


FIG. 3. Once per turntable revolution differential acceleration amplitudes along with the corresponding fits to the galactic basis functions. The mean of each data set has been removed. Each two-day long segment was independently fit. Short gaps in the data were due to local construction activity while the long gap between days 275 and 384 was due to a hardware failure. The right panel shows the histogram of the differential acceleration amplitudes, the bottom panel shows the orientations of the pendulum with respect to the vacuum chamber over the data run. The zoom shows a two-day long segment and its corresponding fit to the galactic basis functions.

Apparatus		
Parameter		Value
Spring Constant	κ	7.1×10^{-10} N m/rad
Quality Factor	Q	$> 1.1 \times 10^5$
Mass of test body set	m	19.4 g
Moment of inertia	I	3.78×10^{-5} kg m ²
Resonant frequency	ω_0	$2\pi \times 0.69$ mHz
Turntable frequency	ω_{TT}	$2\pi \times 0.46$ mHz
Lever-arm	r	1.9 cm
Fiber Length	l	0.94 m

TABLE I. Relevant parameters of the torsion balance. The lever-arm r is the radial distance from the pendulum's fiber axis to the center of mass of each set of test bodies.

Thermal expansion of the feet aligned the turntable rotation axis to local vertical. [15]

The pendulum was built from strictly non-magnetic materials and machined with ceramic tools to avoid ferromagnetic impurities. Additionally, the pendulum was surrounded by three layers of co-rotating magnetic shielding and one non-rotating shield to minimize the effects of external magnetic fields. The inner-most magnetic shield was carefully demagnetized to avoid eddy current damping on the pendulum which preserved the high quality factor and low thermal noise.

To reduce effects of temperature variations, the vacuum chamber was surrounded by a co-rotating sheet metal shield, a concentric lab-fixed shield made of aluminum and insulating foam, and an enclosure made of construction insulation. The torsion fiber was also surrounded by a thermally-isolated thick-walled copper tube. Finally, the experiment was located in an underground laboratory which was temperature controlled to ± 25 mK daily variation with a non-cycling air conditioner.

Analysis - The experiment recorded data from July 7, 2024 to July 7, 2025. We rotated the pendulum 180° with respect to the vacuum chamber on July 31, 2024, February 15, 2025, and May 1, 2025 to reduce systematic effects that may be associated with the pendulum orientation relative to the vacuum chamber (such as tilt and electrostatics). Rotating the pendulum changes the sign of the science signal while maintaining most systematics; these pendulum reorientations were accounted for in the analysis.

The duty cycle of the apparatus was severely restricted due to nearby construction activity and an unexpected hardware failure. Although the data spans 366 days, only 186 days (51%) were free of external disturbances and included in the data set. The measured torsion balance angle was calibrated with a programmed turntable speed change (see Supplementary Material). The angle was converted to differential acceleration by inverting the harmonic oscillator response of the pendulum with a time-domain filter and scaling by the relevant fixed parameters. An additional low-pass filter (1 mHz third-order

Butterworth) was applied to minimize the effect of high frequency noise. We corrected for the response of this filter at the turntable frequency (0.4% attenuation, $\sim 54^\circ$ phase). The differential acceleration time series was split into two turntable-rotation long sets. Each set was fit to a linear combination of sinusoidal functions with frequencies of harmonics of the turntable angle (ω_{TT} , $2\omega_{TT}$, $3\omega_{TT}$, etc.) and harmonics of the torsional resonance (ω_0 , $2\omega_0$, $3\omega_0$, etc.). The full fit function is shown in the Supplementary Material.

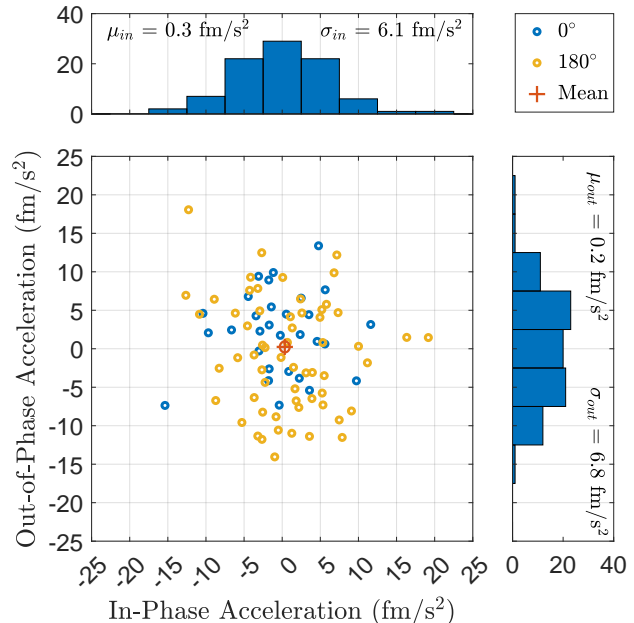


FIG. 4. Measured accelerations from each two-day long segment towards the galactic center (in-phase) and the orthogonal direction (out-of-phase). The blue indicates the points taken at a pendulum orientation of 0° and yellow indicates 180° . The red cross and circle, respectively, indicate the mean and corresponding uncertainty. The top and right panels show the histograms for the in-phase and out-of-phase accelerations, respectively.

The instrument experienced occasional transients due to earthquakes, nearby construction activity and other environmental disturbances. We discarded data sets that fell under two criteria: misfit-squared exceeding the 99th percentile of the corresponding χ^2 -distribution, and a once per turntable-revolution (ω_{TT}) acceleration component outside of the 95th percentile of the component's distribution. We subtracted the mean ω_{TT} -acceleration amplitude of each data set leaving only the time varying components. Figure 3 shows the surviving once per turntable revolution acceleration amplitudes. The ω_{TT} -acceleration was then extracted in two-day long segments. Segments that had less than a quarter of a sidereal day of data were discarded. Each segment was fit to galactic basis functions. These functions consisted of

the location of the center of the Milky Way (RA: 18^{h} Dec: -29°) projected into the horizontal plane of the lab and an orthogonally oriented function. These functions modulate once per sidereal day due to the rotation of the Earth and the location of our lab at $\sim 48^{\circ}$ latitude. The location of the galactic center and the necessary coordinate transformations were computed using the **Astropy** [16] libraries. This fitting yielded 30 points for the 0° pendulum orientation and 60 points for 180° for a total of 90 independent measurements.

Results - The series of measured differential accelerations toward the galactic center is shown in Figure 4. Measuring the out-of-phase component verifies the sensitivity of the experiment as the signal of interest would only appear as a non-zero in-phase component. We take the mean and corresponding uncertainty calculated from the scatter of the measurements to give a final measure of the differential acceleration:

$$\Delta a_{DM,Be-Al} = 0.3 \pm 0.6 \text{ fm/s}^2 \quad (1\sigma) \quad (1)$$

The gravitational acceleration on Earth towards the galactic dark matter is $\geq 50 \text{ pm/s}^2$. [17] If the galactic dark matter causes an acceleration that distinguishes between beryllium and aluminum, the interaction must be smaller than the gravitational acceleration by a factor of:

$$\eta_{DM,Be-Al} \leq 2.6 \times 10^{-5} \quad (95\text{-confidence}). \quad (2)$$

These constraints are a factor of four improvement over previous measurements. [18]

Discussion - This observation can be applied to a variety of theoretical scenarios; many of which depend on the use of different test body materials. We chose to use aluminum and beryllium test bodies to maximize sensitivity to the leading theories (discussed below). Yet, our observations limit any long-range interaction between dark matter and normal matter that does not couple identically to aluminum and beryllium. [17] Other experiments have made different material choices and thus restrict these finely-tuned scenarios as well. [18]

There is no underlying symmetries in the Standard Model that require conservation of baryon number (B) and lepton number (L). [19–22] Yet, global violation of these conservations have not been observed. This has led to speculation that there may exist a B- or L-dependent fifth force. Such fifth forces have been stringently tested for normal matter. [23] Our results extend these tests to include dark matter-normal matter interactions.

Grand Unified Theories [24] attempt to unify the electromagnetic, weak, and strong forces of nature into a single force. In many of these theories, B and L numbers are not conserved; instead the difference (B-L) is the conserved quantity. [25, 26] This conservation has many possible consequences for dark matter including dark matter having B-L charge. [27, 28] Our experiment is uniquely designed to search for interactions to this B-L

charged dark matter; the test body materials were chosen to maximize their difference in B-L charge. There is ambiguity in what B-L charge dark matter could have. Regardless, our results restrict the strength of such an interaction.

There are a lacking number of dedicated tests of quantum gravity theories. Despite this, we can test a few aspects of quantum gravity in laboratory experiments including the Weak Gravity Conjecture. [29, 30] A statement of the conjecture is that gravity has to be the weakest force of nature to have a consistent theory of quantum gravity. Our observations show that the conjecture is still valid for interactions between dark matter and normal matter.

The Equivalence Principle is a foundational aspect of our geometric understanding of gravity (i.e. General Relativity). The principle states that gravity is independent of the composition of objects. This have been tested extensively for a variety of materials and distance scales. [18, 23] However, these tests use normal matter as the source mass making them blind to any violation associated with dark matter. Our results directly test the Equivalence Principle towards dark matter at galactic scales and set limits on the Eötvös parameter for beryllium and aluminum towards dark matter ($\eta_{DM,Be-Al}$ in Equation 2).

Conclusion - We constructed a rotating torsion balance to search for a long-range interaction between normal matter and dark matter. We observe no evidence for such an interaction and set strict limits on its possible strength. Although this constrains a variety of theoretical possibilities for dark matter, our observation is model independent. Any proposed dark matter interaction that does not couple identically to beryllium and aluminum is constrained by this observation.

There are very few laboratory experiments that directly probe dark matter without assuming a theoretical model. Our experiment achieved this on a galactic scale while being located on Earth. This observation furthers our understanding of not just dark matter but also the nature of gravity and fundamental symmetries of the universe.

Data Availability - Raw data will be shared upon request. The fit amplitudes and analysis code can be found at <https://github.com/EotWash/EP-Analysis>.

Acknowledgements - This work was supported by funding from the NSF under Awards PHY-1607385, PHY-1607391, PHY-1912380, and PHY-1912514.

-
- [1] Paolo Salucci. The distribution of dark matter in galaxies. *The Astronomy and Astrophysics Review*, 27(1):2, 2019.
 - [2] DES Collaboration. The Dark Energy Survey: Cosmology Results with 1500 New High-redshift Type Ia

- Supernovae Using the Full 5 yr Data Set. *The Astrophysical Journal Letters*, 973(1):L14, oct 2024. doi: 10.3847/2041-8213/ad6f9f. URL <https://dx.doi.org/10.3847/2041-8213/ad6f9f>.
- [3] DESI Collaboration. DESI DR2 Results II: Measurements of Baryon Acoustic Oscillations and Cosmological Constraints. *arxiv*, 2025. URL <https://arxiv.org/abs/2503.14738>.
- [4] Planck Collaboration. Planck 2018 results - I. Overview and the cosmological legacy of Planck. *A&A*, 641:A1, 2020. doi:10.1051/0004-6361/201833880. URL <https://doi.org/10.1051/0004-6361/201833880>.
- [5] Jason A.S. Hunt and Eugene Vasiliev. Milky way dynamics in light of gaia. *New Astronomy Reviews*, 100:101721, 2025. ISSN 1387-6473. doi: <https://doi.org/10.1016/j.newar.2024.101721>. URL <https://www.sciencedirect.com/science/article/pii/S1387647324000289>.
- [6] Stefan Payne-Wardenaar ESA/Gaia/DPAC. The best Milky Way map, by Gaia (edge-on). 2025. URL https://www.esa.int/ESA_Multimedia/Images/2025/01/The_best_Milky_Way_map_by_Gaia_edge-on.
- [7] Gianfranco Bertone. *Particle dark matter: observations, models and searches*. Cambridge University Press, 2010.
- [8] Giorgio Arcadi, Maíra Dutra, Pradipta Ghosh, Manfred Lindner, Yann Mambrini, Mathias Pierre, Stefano Profumo, and Farinaldo S Queiroz. The waning of the wimp? a review of models, searches, and constraints. *The European Physical Journal C*, 78:1–57, 2018.
- [9] Nassim Bozorgnia, Joseph Bramante, James M. Cline, David Curtin, David McKeen, David E. Morrissey, Adam Ritz, Simon Viel, Aaron C. Vincent, and Yue Zhang. Dark matter candidates and searches. *Canadian Journal of Physics*, 2024. ISSN 0008-4204. doi:<https://doi.org/10.1139/cjp-2024-0128>. URL <https://www.sciencedirect.com/science/article/pii/S0008420424000692>.
- [10] Pablo Villanueva-Domingo, Olga Mena, and Sergio Palomares-Ruiz. A brief review on primordial black holes as dark matter. *Frontiers in Astronomy and Space Sciences*, Volume 8 - 2021, 2021. ISSN 2296-987X. doi:10.3389/fspas.2021.681084. URL <https://www.frontiersin.org/journals/astronomy-and-space-sciences/articles/10.3389/fspas.2021.681084>.
- [11] A. Boyarsky, M. Drewes, T. Lasserre, S. Mertens, and O. Ruchayskiy. Sterile neutrino dark matter. *Progress in Particle and Nuclear Physics*, 104:1–45, 2019. ISSN 0146-6410. doi:<https://doi.org/10.1016/j.pnpnp.2018.07.004>. URL <https://www.sciencedirect.com/science/article/pii/S0146641018300711>.
- [12] E.G. Adelberger, J.H. Gundlach, B.R. Heckel, S. Hoedl, and S. Schlamminger. Torsion balance experiments: A low-energy frontier of particle physics. *Progress in Particle and Nuclear Physics*, 62(1):102–134, 2009. ISSN 0146-6410. doi:<https://doi.org/10.1016/j.pnpnp.2008.08.002>. URL <https://www.sciencedirect.com/science/article/pii/S0146641008000720>.
- [13] EA Shaw, MP Ross, CA Hagedorn, EG Adelberger, and JH Gundlach. Torsion-balance search for ultralow-mass bosonic dark matter. *Physical Review D*, 105(4):042007, 2022.
- [14] Peter R. Saulson. Thermal noise in mechanical experiments. *Phys. Rev. D*, 42:2437–2445, Oct 1990. doi: 10.1103/PhysRevD.42.2437. URL <https://link.aps.org/doi/10.1103/PhysRevD.42.2437>.
- [15] Erik A Shaw. *Equivalence Principle Tests and Direct Searches for Ultra-Light Dark Matter with Fused-Silica Torsion Fibers*. University of Washington, 2023.
- [16] Astropy Collaboration and Astropy Project Contributors. The Astropy Project: Sustaining and Growing a Community-oriented Open-source Project and the Latest Major Release (v5.0) of the Core Package. *Astrophys. J.*, 935(2):167, August 2022. doi:10.3847/1538-4357/ac7c74.
- [17] Christopher W. Stubbs. Experimental limits on any long range nongravitational interaction between dark matter and ordinary matter. *Phys. Rev. Lett.*, 70:119–122, Jan 1993. doi:10.1103/PhysRevLett.70.119. URL <https://link.aps.org/doi/10.1103/PhysRevLett.70.119>.
- [18] Todd A Wagner, Stephan Schlamminger, Jens H Gundlach, and Eric G Adelberger. Torsion-balance tests of the weak equivalence principle. *Classical and Quantum Gravity*, 29(18):184002, 2012.
- [19] Leah J Broussard et al. Baryon number violation: from nuclear matrix elements to BSM physics. *Journal of Physics G: Nuclear and Particle Physics*, 52(8):083001, aug 2025. doi:10.1088/1361-6471/adf081. URL <https://dx.doi.org/10.1088/1361-6471/adf081>.
- [20] P S B Dev et al. Searches for baryon number violation in neutrino experiments: a white paper. *Journal of Physics G: Nuclear and Particle Physics*, 51(3):033001, jan 2024. doi:10.1088/1361-6471/ad1658. URL <https://dx.doi.org/10.1088/1361-6471/ad1658>.
- [21] Pavel Fileviez Perez, Andrea Pocar, KS Babu, Leah J Broussard, Vincenzo Cirigliano, Susan Gardner, Julian Heeck, Ed Kearns, Andrew J Long, Stuart Raby, et al. On baryon and lepton number violation. *arXiv preprint arXiv:2208.00010*, 2022.
- [22] Yi Cai, Tao Han, Tong Li, and Richard Ruiz. Lepton number violation: Seesaw models and their collider tests. *Frontiers in Physics*, Volume 6 - 2018, 2018. ISSN 2296-424X. doi:10.3389/fphy.2018.00040. URL <https://www.frontiersin.org/journals/physics/articles/10.3389/fphy.2018.00040>.
- [23] Pierre Touboul et al. *MICROSCOPE* Mission: Final Results of the Test of the Equivalence Principle. *Phys. Rev. Lett.*, 129:121102, Sep 2022. doi: 10.1103/PhysRevLett.129.121102. URL <https://link.aps.org/doi/10.1103/PhysRevLett.129.121102>.
- [24] W De Boer. Grand unified theories and supersymmetry in particle physics and cosmology. *Progress in Particle and Nuclear Physics*, 33:201–301, 1994. ISSN 0146-6410. doi:[https://doi.org/10.1016/0146-6410\(94\)90045-0](https://doi.org/10.1016/0146-6410(94)90045-0). URL <https://www.sciencedirect.com/science/article/pii/0146641094900450>.
- [25] W. Buchmüller, C. Greub, and P. Minkowski. Neutrino masses, neutral vector bosons and the scale of B-L breaking. *Physics Letters B*, 267(3):395–399, 1991. ISSN 0370-2693. doi:[https://doi.org/10.1016/0370-2693\(91\)90952-M](https://doi.org/10.1016/0370-2693(91)90952-M). URL <https://www.sciencedirect.com/science/article/pii/037026939190952M>.
- [26] Lorenzo Basso, Alexander Belyaev, Stefano Moretti, and Claire H. Shepherd-Themistocleous. Phenomenology of the minimal $B - L$ extension of the standard model: Z' and neutrinos. *Phys. Rev. D*, 80:055030, Sep 2009. doi: 10.1103/PhysRevD.80.055030. URL <https://link.aps.org/doi/10.1103/PhysRevD.80.055030>.

- [27] Werner Rodejohann and Carlos E. Yaguna. Scalar dark matter in the B-L model. *Journal of Cosmology and Astroparticle Physics*, 2015(12):032, dec 2015. doi:10.1088/1475-7516/2015/12/032. URL <https://dx.doi.org/10.1088/1475-7516/2015/12/032>.
- [28] Jun Guo, Zhaofeng Kang, P. Ko, and Yuta Orikasa. Accidental dark matter: Case in the scale invariant local $B - L$ model. *Phys. Rev. D*, 91:115017, Jun 2015. doi:10.1103/PhysRevD.91.115017. URL <https://link.aps.org/doi/10.1103/PhysRevD.91.115017>.
- [29] Daniel Harlow, Ben Heidenreich, Matthew Reece, and Tom Rudelius. Weak gravity conjecture. *Rev. Mod. Phys.*, 95:035003, Sep 2023. doi:10.1103/RevModPhys.95.035003. URL <https://link.aps.org/doi/10.1103/RevModPhys.95.035003>.
- [30] Nima Arkani-Hamed, Luboš Motl, Alberto Nicolis, and Cumrun Vafa. The string landscape, black holes and gravity as the weakest force. *Journal of High Energy Physics*, 2007(06):060, jun 2007. doi:10.1088/1126-6708/2007/06/060. URL <https://dx.doi.org/10.1088/1126-6708/2007/06/060>.

SUPPLEMENTARY MATERIAL

Fit Functions - The observed differential acceleration was fit to the following linear combination of sinusoidal functions with frequencies of harmonics of the turntable angle (ω_{TT} , $2\omega_{TT}$, $3\omega_{TT}$, etc.) and harmonics of the torsional resonance (ω_0 , $2\omega_0$, $3\omega_0$, etc.):

$$\begin{aligned} \Delta a = & a_{TT} \cos(\omega_{TT}t) + b_{TT} \sin(\omega_{TT}t) \\ & + a_{2TT} \cos(2\omega_{TT}t) + b_{2TT} \sin(2\omega_{TT}t) \\ & + a_{3TT} \cos(3\omega_{TT}t) + b_{3TT} \sin(3\omega_{TT}t) \\ & + a_{4TT} \cos(4\omega_{TT}t) + b_{4TT} \sin(4\omega_{TT}t) \\ & + a_{5TT} \cos(5\omega_{TT}t) + b_{5TT} \sin(5\omega_{TT}t) \\ & + a_1 \cos(\omega_0t) + b_1 \sin(\omega_0t) \\ & + a_2 \cos(2\omega_0t) + b_2 \sin(2\omega_0t) \\ & + a_3 \cos(3\omega_0t) + b_3 \sin(3\omega_0t) \\ & + a_4 \cos(4\omega_0t) + b_4 \sin(4\omega_0t) \\ & + a_5 \cos(5\omega_0t) + b_5 \sin(5\omega_0t) \\ & + K \end{aligned}$$

where a_i and b_i are the harmonic fit parameters, t is time, K is the offset fit parameter.

The once per turn table revolution amplitudes, a_{TT} and b_{TT} , were combined into a single complex number $a_{TT} + ib_{TT}$ whose amplitude is shown in Figure 3. These were then fit to the galactic basis functions, z_{in} and z_{out} via:

$$a_{TT} + ib_{TT} = (\alpha + i\beta) \left(z_{in}(t) + iz_{out}(t) \right) \quad (3)$$

to give the in-phase and out-of-phase amplitudes α and β , respectively. The use of complex numbers allows the phases of the various signals to be readily accounted for.

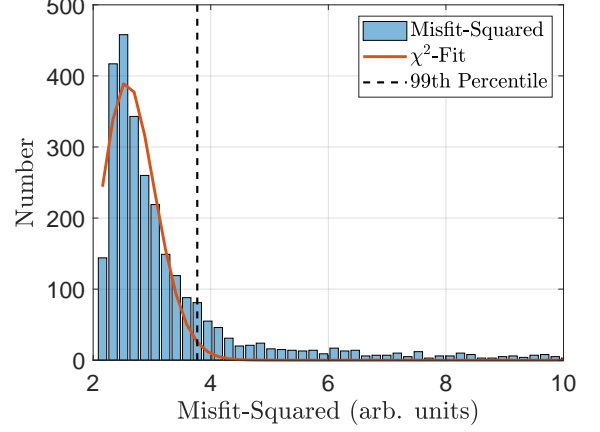


FIG. 5. Misfit-squared, fit to a χ^2 distribution, and 99th-percentile cutoff.

χ^2 -Cuts - We discarded data that was contaminated by external disturbances. To do this, we fit the misfit-squared of the data sets to a χ^2 -distribution, shown in Figure 5. The 99th-percentile of this distribution was then used as a cutoff. Any data set whose misfit-squared was greater than this was discarded.

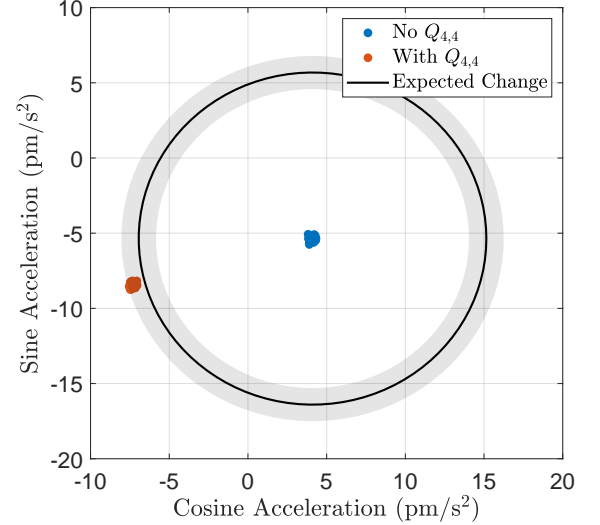


FIG. 6. Extracted $4\omega_{TT}$ accelerations with and without the gravitational $Q_{4,4}$ masses along with the expected change in amplitude.

Gravitational Cross-check - The torsion pendulum had a significant q_{44} moment due to its geometry. We utilized this moment to cross-check the acceleration sensitivity of the apparatus. A set of four 1.35 kg brass masses were placed in-plane with the pendulum at a radius of 28.6 cm in a four fold symmetric pattern. This induced a known external Q_{44} . The coupling between the induced Q_{44} and the pendulum's q_{44} produced an acceleration at $4\omega_{TT}$.

The measurement of the $4\omega_{TT}$ acceleration with and without the injected Q_{44} is shown in Figure 6 along with the expected change in $4\omega_{TT}$ acceleration. The environment had a Q_{44} without the injection and the phase change was not well controlled. Thus the expected signal is a ring of fixed amplitude around the environmental $4\omega_{TT}$ acceleration.

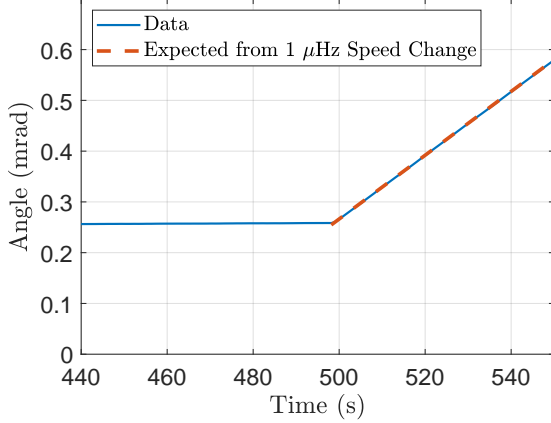


FIG. 7. Autocollimator angle readings during a 1 μHz turntable speed change. This speed change allows the angle calibration to be cross-checked with the turntable.

Inertial Calibration - The air-bearing turntable's rotation rate was determined with high fidelity by a set of optical rotary encoders. The autocollimator was rigidly attached to the vacuum chamber which was rotated by the turntable. The pendulum had a relatively long inertial response to changes in the speed of the turntable. We utilized this to calibrate the angular readout relative to the turntable speed.

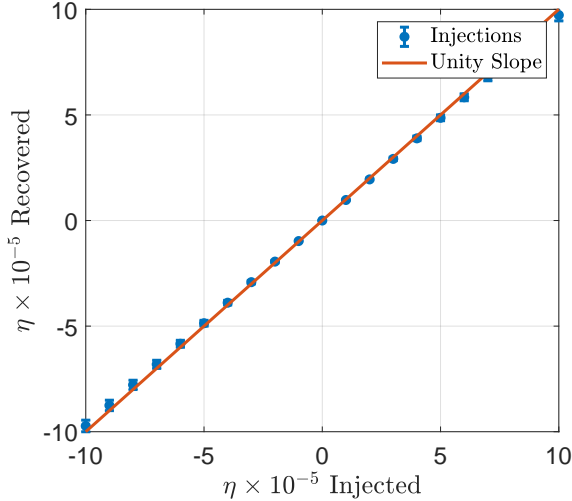


FIG. 8. False dark matter signal injection and extraction.

When the turntable undergoes a step change in speed, the pendulum stays inertial while the autocollimator begins to rotate. This initially appears as a linear angle change whose slope depends on the step change amplitude as shown in Figure 7

Signal Injection - We conducted a set of artificial signal injections through our analysis to ensure accurate extraction of a non-zero η . These were done from $\eta = -10^{-4}$ to 10^{-4} in 10^{-5} steps. The results of this injection are shown in Figure 8.

This shows accurate extraction of the signal across a wide selection of η values. The slight non-linear behavior at large injection amplitudes is due to the statistical cuts removing the peaks of the injected signal. This behavior is eliminated by increasing the misfit threshold.

Tilt Coupling - The tilt of the apparatus relative to local vertical can introduce false once per revolution signals. We employed a control system to minimize this effect. However, residual tilts may effect our results.

We conducted a series of tilt injections to place bounds on this effect. The tilt was injected by oscillating the temperature of one of the thermal expansion feet at 0.57 mHz. The resultant tilt and apparent differential acceleration were then compared to get a coupling from tilt to acceleration.

This coupling can differ from tilt direction and pendulum mirror. We measured the coupling of each mirror used in the science data (0° and 180°) for each tilt direction (A and B)

$$K_{0^\circ, A} = 6.3 \pm 0.3 \text{ nm/s}^2/\text{rad}$$

$$K_{0^\circ, B} = 25.2 \pm 0.5 \text{ nm/s}^2/\text{rad}$$

$$K_{180^\circ, A} = 28.2 \pm 1.1 \text{ nm/s}^2/\text{rad}$$

$$K_{180^\circ, B} = 24.4 \pm 0.5 \text{ nm/s}^2/\text{rad}$$

The apparatus tilts ~ 4.7 mrad per day. Using this, we place an upper limit of the possible tilt induced differential acceleration of $\Delta a_{\text{tilt}} \leq 0.3 \text{ fm/s}^2$ ($\eta_{\text{tilt}} \leq 0.6 \times 10^{-5}$).

Magnetic Coupling - The influence of external magnetic fields is significantly reduced by the magnetic shielding. We conducted a set external of magnetic injections to place limits on the residual influence. This consisted of placing large coils around the apparatus through which an oscillating current was driven at 0.57 mHz. A large external field of 70 μG showed no influence on the pendulum. With this non-observation, we can set an upper limit on the magnetic coupling of $0.14 \text{ nm/s}^2/\text{G}$ and a maximum magnetic systematic of $\Delta a_{\text{mag}} \leq 1.1 \times 10^{-3} \text{ fm/s}^2$ ($\eta_{\text{mag}} \leq 0.006 \times 10^{-5}$).

Gravity Gradient Coupling - The design of the pendulum minimizes its gravitational moments. We measured the residual $q_{2,1}$ moment by rotating the exterior $Q_{2,1}$ compensating masses by 180° . This yielded a $q_{2,1} = 0.03 \text{ g/cm}^2$.